A permanent Magnet to search for long-lived $\pi^+\pi^-$ atoms

S.Aogaki[1], M.Chiba[2], Iwashita[3] , M.Kobayashi[4], K.Okada[1] and F.Takeutchi[1]

1. Kyoto-Sangyo University , 2. Tokyo Metropolitan University, 3. Kyoto University, 4. KEK

Dirac collaboration

4 September, 2011

1. Introduction

The DIRAC experiment [1] has been running at CERN PS measuring lifetimes of $\pi^+\pi^-$, $K^+\pi^-$ and π^+K^- atoms by a two arm spectrometer at CERN PS as shown in Fig. 1. Up to now more than 21,000 $\pi^+\pi^-$ pairs originated from the $\pi^+\pi^-$ atom ($A_{2\pi}$) breakup were identified and the overall accuracy of the $A_{2\pi}$ lifetime is about 9% in accordance with the DIRAC proposal.

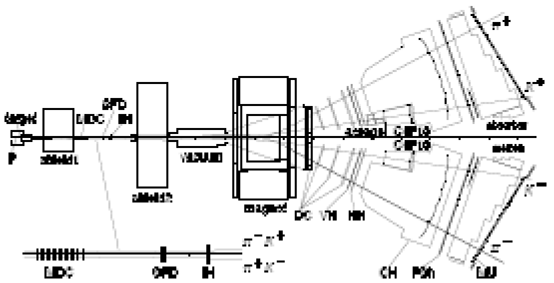

Figure 1: *Dirac setup: MDC are microdrift gas chambers, SFD is a scintillating fiber detector and IH is a scintillation ionization hodoscope. Downstream the spectrometer magnet there are drift chambers (DC), vertical (VH) and horizontal (HH) scintillation hodoscopes, Cherenkov detectors containing nitrogen (CH), heavy gas C_4F_{10} and aerogel radiatiors, shower detectors (PSh) and scintillation muon detectors (MU).*

A new DIRAC proposal [2] was presented to measure long-lived $\pi^+\pi^-$ atoms at CERN PS. This measurement allows to extract the difference $|a_0 - a_2|$ of *s*-wave $\pi\pi$-scattering length with accuracy of 4.3%. In addition, the observation of long-lived (metastable) $A_{2\pi}$ states will be performed with the same setup. This observation opens a possibility to measure the energy difference between *ns* and *np* states and to determine the value of another combination $2a_0 + a_2$ of $\pi\pi$ scattering length in a model-independent way. In combination with the first measurement it allows to get a_0 and a_2 separately. The long long-lived $\pi^+\pi^-$ atoms are generated at the Be target and broken up at the the Pt foil as shown in Fig. 2. The distance between the Be target and the Pt foil was chosen to be 100 mm for excluding interaction of the primary beam halo with the Pt foil.

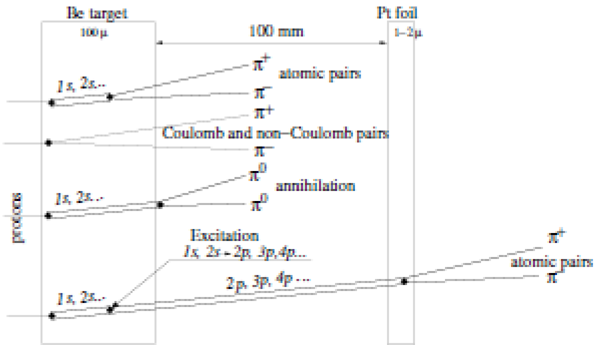

Figure 2: *The long long-lived $\pi^+\pi^-$ atoms are generated at the Be target and broken up at the the Pt foil.*

Simulation of “experimental data” has been performed adding the contributions of simulated : atomic pairs from long-lived atoms produced in the Platinum foil, atomic pairs from the Beryllium target , “Coulomb pairs”, “non-Coulomb pairs” and accidentals. Fig. 3 presents the distribution of simulated data over the *Y* projection of relative momentum *Q*. The cuts on $|Q_X| < 1$ MeV/c and $|Q_L| < 1$ MeV/c have been applied. The quantity Q_T, Q_L, Q_X and Q_Y is the transverse, longitudinal, X and Y components of the relative momentum Q in the atomic pair c.m.s. Simulation shows that in each projection such criterion selects more than 90% of “atomic pairs” from long-lived atoms. Hatched area is a sum of all pairs produced in Beryllium target and light area corresponds to “atomic pairs” from long-lived atoms broken in the Platinum foil.

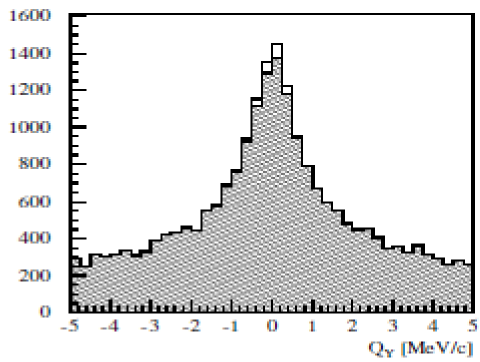

Figure 3: *Simulated distribution of $\pi^+\pi^-$ pairs over Q_Y with criteria: $|Q_X| < 1$ MeV/c, $|Q_L| < 1$ MeV/c. “Atomic pairs” from long-lived atoms (light area) above background produced in Beryllium target (hatched area)*

The signal-to-background ratio is small. It can be improved by installation of an additional retractable magnet which induces the horizontal magnetic field in the gap between Be target and Pt foil. A magnet with the bending power of 0.01 Tm (Tesla*meter) would shift the Q_Y value by 6 MeV/c only for the pairs produced in the Be target leaving unchanged the Q_Y distribution of the pairs produced in the Pt foil. The magnet with such characteristics is installed (see Fig. 4).

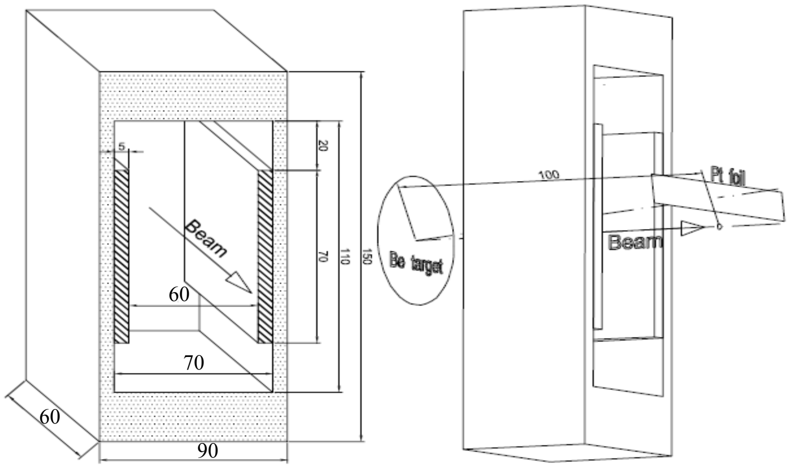

Figure 4: *Permanent magnet dimensions and arrangement of the Beryllium target, permanent magnet and Platinum foil.*

Fig. 5 shows the resulting Q_Y distribution with the improved signal-to-background ratio. We could discriminate the atomic pairs from the background easier than in Fig. 3.

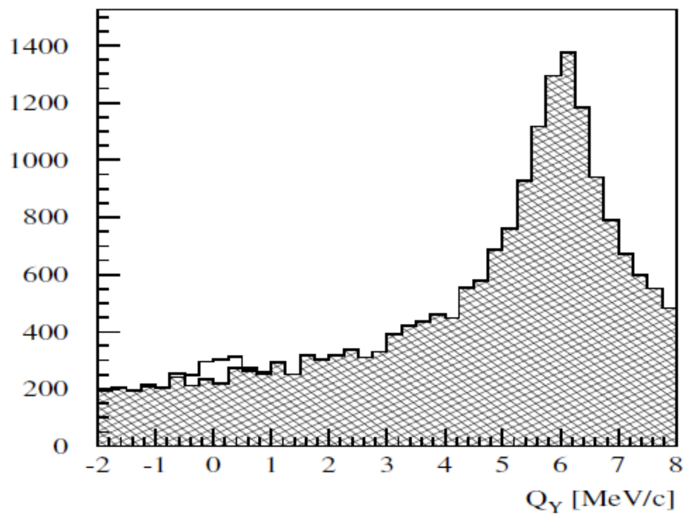

Figure 5: *Simulated distribution of $\pi^+\pi^-$ pairs over Q_Y with criteria:* $|Q_X| < 1$ *MeV/c,* $|Q_L| < 1$ *MeV/c. Additional magnet is implemented. "Atomic pairs" from long-lived atoms (light area) above*

background produced in Beryllium target (hatched area).

A new sample of simulated data with the additional magnet has been fitted with the sum of the distributions of atomic pairs from long-lived atoms, “Coulomb pairs” and “non-Coulomb pairs”. The atomic pairs produced in the Be target with the Q_Y about 6MeV/c are absent in the fit region.
The fit results for distribution over Q_L (with cut $Q_T < 1$ MeV/c) are presented in Fig. 6.

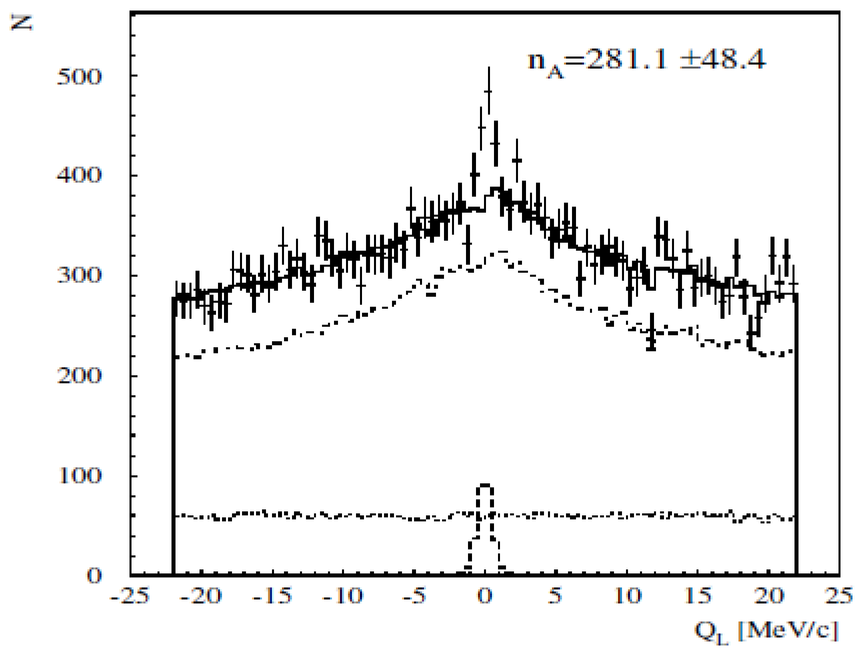

Figure 6: *Simulated distribution of $\pi^+\pi^-$ pairs over Q_L, with criterion $Q_T < 1$ MeV/c. “Experimental” data (points with error bars) are fitted by a sum of “atomic pairs” from longlived states (dashed line), “Coulomb pairs” (by dotted-dashed line), “non-Coulomb pairs” (dotted line). The background sum is shown by the solid line.*

Number of atomic pairs are found to be:

$$n_A^l = 281 \pm 48 \qquad (1)$$

Analysis of the experimental data accounting widths of the atomic pairs distribution over different components of the relative momentum Q allows to find the variable F which provides the distribution of atomic pairs with the best signal-to-background ratio:

$$F = \sqrt{\left(\frac{Q_x}{0.50}\right)^2 + \left(\frac{Q_Y}{0.32}\right)^2 + \left(\frac{Q_L}{0.56}\right)^2} \qquad (2)$$

Here 0.50, 0.32 and 0.56 in units of Mev/c are RMSs of the atomic pairs distribution over corresponding components of the relative momentum Q.

Fig. 7 presents results of analysis for distribution of $\pi^-\pi^-$ pairs over F. We find excess events of the atomic pairs over the solid line at F< 3 MeV/c. It provides a greater number of found atomic pairs due to the weaker cut on Q_T < 2 MeV/c and a better signal-to-error ratio:

$$n_A^l = 327 \pm 37 \qquad (3)$$

$$\frac{n_A}{\partial_{n_A}} = 8.8 \qquad (4)$$

It is worth noting that the simulated number n_A^l is 310.

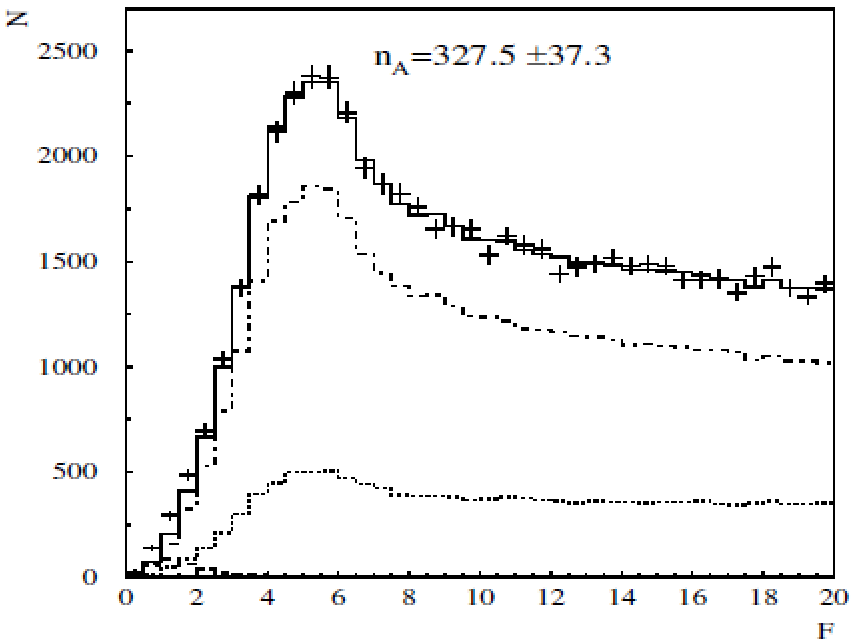

Figure 7: *Simulated distribution of $\pi^-\pi^-$ pairs over F, with criterion Q_T < 2 MeV/c. "Experimental" data (points with error bars) are fitted by a sum of "atomic pairs" from longlived states (dashed line), "Coulomb pairs" (by dotted-dashed line), "non-Coulomb pairs" (dotted line). The background sum is shown by the solid line.*

In order to declare an observation of long-lived $\pi^-\pi^-$ atoms it is needed to achieve a ratio between signal and error greater than 5. The current simulation provides the ratio of 8.8. This means that probability to observe long-lived $\pi^-\pi^-$ atoms is close to 100%.

In the approach without the additional permanent magnet the accuracy of effect separation will be worse. At equal conditions the simulated number of reconstructed atomic pairs is

$$n_A^l = 334 \pm 89 \qquad (5)$$

To achieve the value of 5 in the signal-to-error ratio, required for the observation, the needed statistic should be increased by 1.8 that can be accomplished with a high efficiency of the event reconstruction and/or a longer run time.

2. Permanent magnet

We had experienced to fabricate a small analyzing magnet consist of neodymium [3] to get better separation of π^+ and π^- tracks broken from an $\pi^+\pi^-$ atom in scintillation fiber detectors [4] set between the production target and the main analyzing magnet in the Dirac spectrometer [5]. We utilized a permanent magnet to realize the required-measuring conditions. The magnet should be installed in the vacuum target station just after the production target made of Beryllium in Fig. 1 where the primary-proton beam delivered from CERN PS passing through. The beam with the halos should pass through without hit the magnet. The magnet is set between the production target and the Platinum foil where the atomic pairs are broken as in Fig.4. The distance is determined to be 10cm so that most of the long-lived atomic pairs are alive. The magnetic field strength should not much higher than 0.1T not to quench the p or d states of the atoms to the s state since the quench effect is proportional to the square of the field strength as long as the enough bending power of BL of 0.01 Tm to move aside the peak of the short-lived $\pi^+\pi^-$ pairs in Q_Y as shown in Fig. 5. At and after the breaking target the magnetic field should be low enough not to bend the charged pions broken from $\pi^+\pi^-$ atoms.

We utilize a permanent magnet to realize the required conditions. Permanent magnet has advantages over electromagnets. It does not need an electric current to magnetize which generates heat in the vacuum setting. The magnetic field is stable since there is no thermal and mechanical change due to the electric current. But it is reported that the magnetic field strength would decrease due to strong irradiations from protons and neutrons, on the other hand the degradation seems rather weak for gamma rays [6 - 8]. We should keep a watch on it in the radiation environment.

We made a permanent magnet as shown in Figs.8 and 9. A couple of neodymium pieces of 70x60 mm^2 with the thickness of 5 mm were employed. The gap is 60 mm and the integrated magnetic field along the beam is around 0.01 Tm. The external sizes of the magnet are 150 mm wide, 80 mm high and 60 mm deep. Two permanent magnet poles are glued on the inner facing surfaces of the iron frame. The dimensions of the permanent magnets are 70 mm x 60 mm x 5 mm. The gap distance between the two magnets is 60 mm. Each permanent magnet is composed of a piece of 70 mm x 40 mm, two pieces of 30 mm x 20 mm, and a piece of 20 mm x 10 mm, as shown in Fig. 9. The permanent magnet material of the largest plates is N35 and that of the rest is N40, where the remanent field Br of N40 and N35 are specified as 1.22~1.25T and 1.17~1.22 T, respectively. The leg thickness of the iron frame is 20mm and the thickness of the top and bottom plate is 10mm. The iron frame is made of structural mild steel, which should correspond to SS 400. Because the magnetic field in the gap is not generated by the iron part but the permanent magnets, the field should not be much affected by the difference of irons, as long as it has enough high permeability.

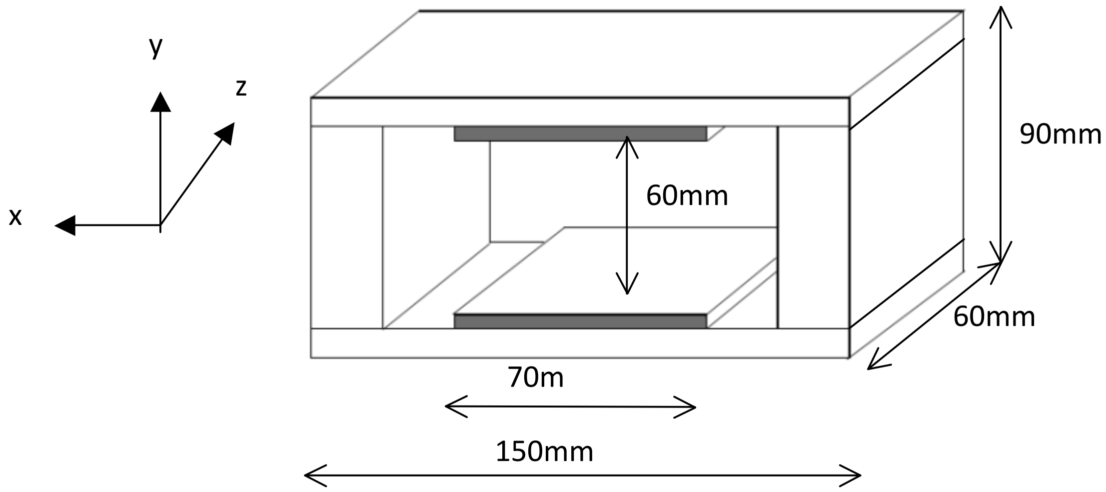

Figure 8: *A drawing of the permanent magnet with the axes of the coordinates*

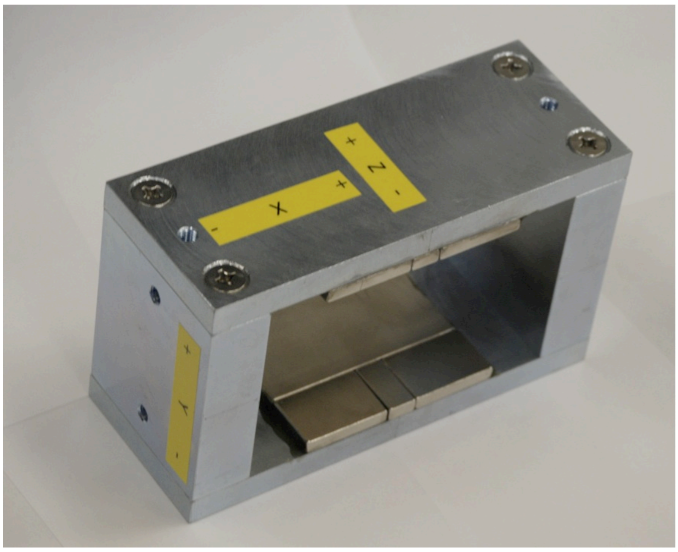

Figure 9: *A picture of the permanent magnet. The directions of + and - for the X coordinate labeled on the surface should be reversed. The right-handed coordinate system is employed as shown in Fig. 8.*

3. Magnetic field simulation

RADIA version 4.29[9-11] is used for the magnetic field calculation. The calculated geometry is shown in Fig. 10, where the permanent magnet plate dimensions are 5mm in thickness, 60mm in length and 70mm in width. The coordinate system is shown in the figure, where the origin is coincides with the centroid of the magnet. In the calculation, three symmetries are used: x-y plane, y-z plane, and z-x plane, which reduces the system 1/8 comparing with the full system. The remanent flux density of the magnet is assumed to be 1.22T and the recoil permeability of 1.05. The return yoke material is "steel37" equipped in RADIA, which is an inexpensive steel with C<0.13%.

The resulted field map of By is shown in Table 1. Since the assumption may not reflect the real situation, the result is scaled to match the measured value at the origin (0,0,0), where the factor was 0.983. This value seems good for this kind of calculation.

Figure 11 shows the y-component of the magnetic flux density along z on x=y=0 line and x=y=10. The integrated values on these lines are as follows:

$$\int_{0mm}^{100mm} By_{x=0,y=0}(z)\,dz = 0.00490\,[\mathrm{T.m}], \quad \int_{0mm}^{100mm} By_{x=10,y=10}(z)\,dz = 0.00492\,[\mathrm{T.m}], \qquad (6)$$

where only the half of the region is counted along the path. The x-component and y-component along x=y=10mm line are shown in Fig. 12,

$$\int_{0mm}^{100mm} Bx_{x=10,y=10}(z)\,dz = 0.316\,[\mathrm{mT.m}], \quad \int_{0mm}^{100mm} Bz_{x=10,y=10}(z)\,dz = 1.297\,[\mathrm{mT.m}]. \qquad (7)$$

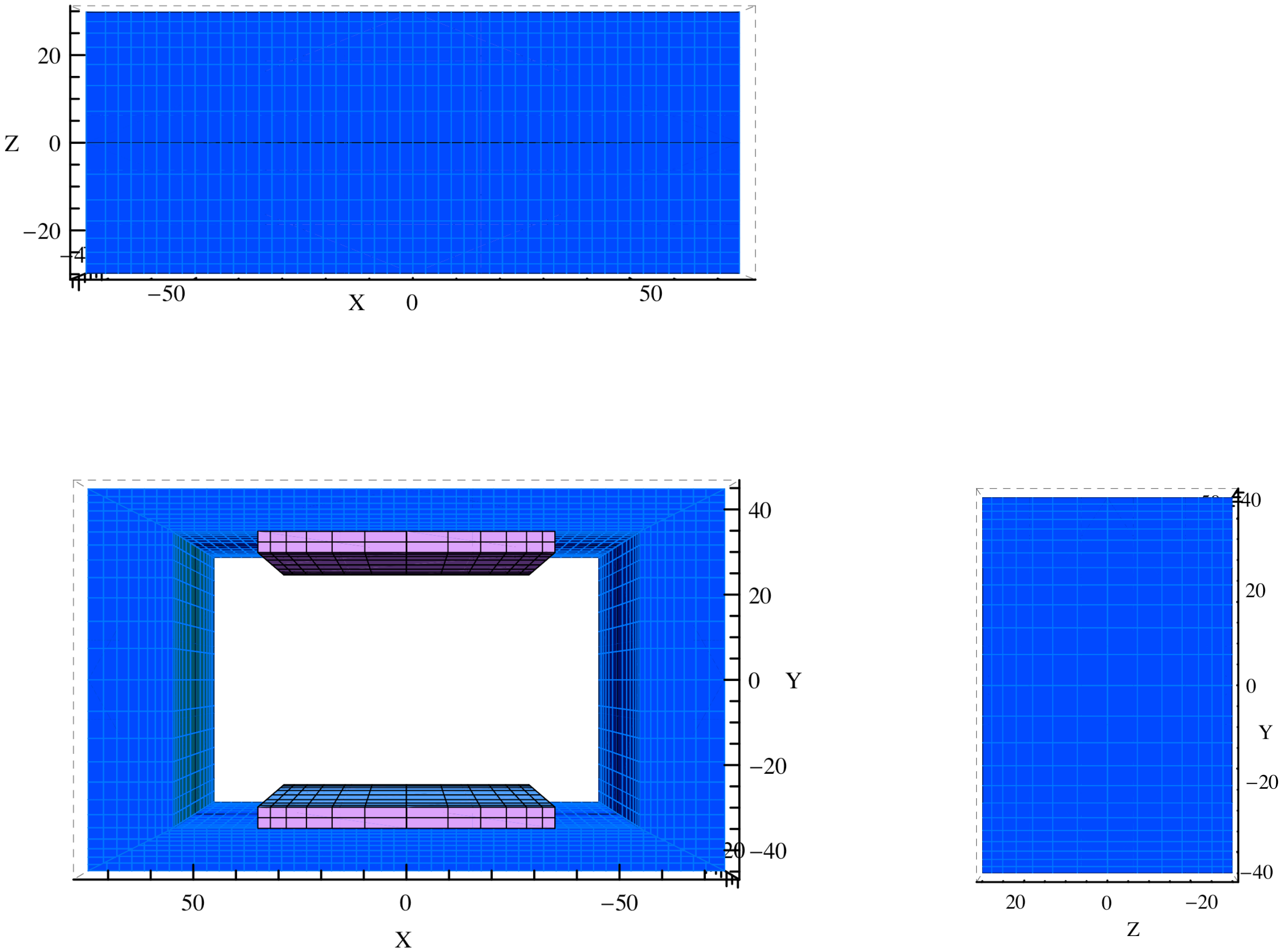

Fig. 10: *Calculated geometry, the unit is in mm: Top View, Front view and side view.*

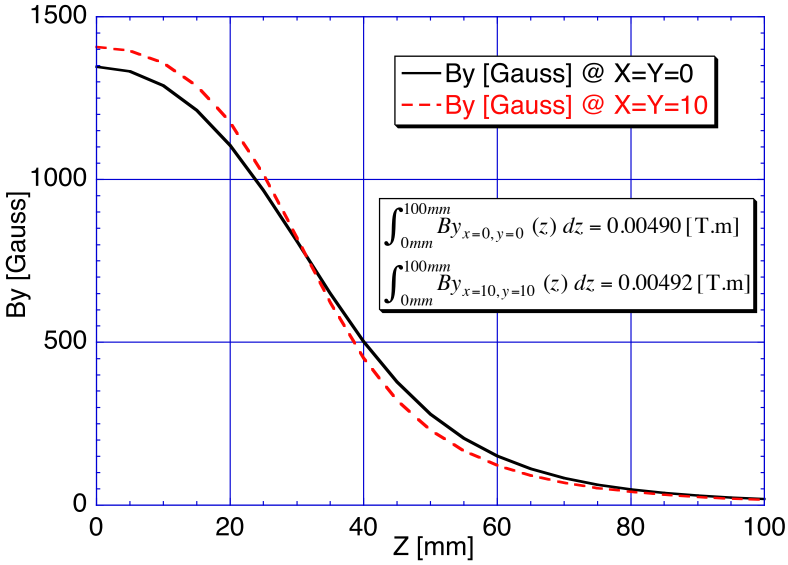

Fig. 11: *Calculated By distributions on lines of x=y=0 and x=y=10mm.*

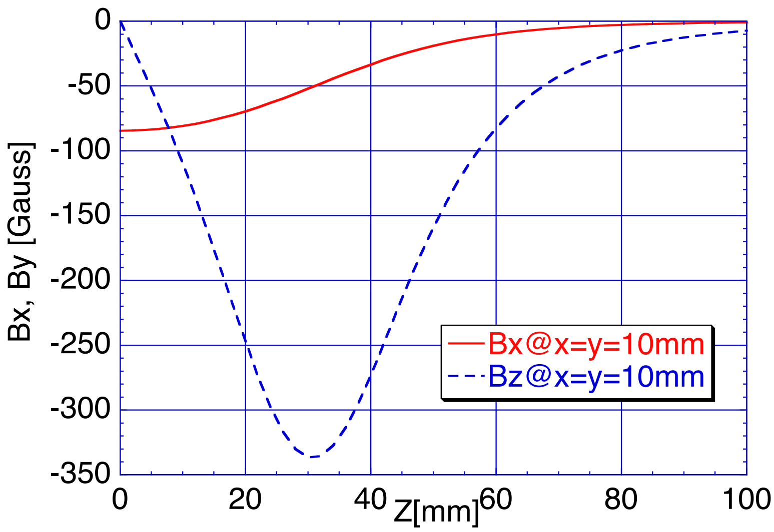

Fig. 12: *Calculated Bx and Bz distributions on line x=y=10mm.*

Table 1: *The field map calculated by RADIA. The values are scaled to match the measured value, where the factor was 0.983.   Units are in Gauss and mm.*

y=0	x=0	x=2	x=4	x=6	x=8	x=10	x=12	x=14	x=16	x=18	x=20
z=0	1323	1321	1316	1308	1296	1280	1260	1235	1206	1172	1133
z=5	1309	1307	1302	1294	1282	1266	1246	1222	1193	1160	1121
z=10	1266	1264	1260	1252	1240	1225	1206	1182	1154	1122	1084
z=15	1192	1190	1186	1178	1168	1153	1135	1113	1087	1056	1021
z=20	1086	1084	1080	1073	1063	1050	1034	1014	990	962	930
z=25	950	949	946	939	931	919	905	887	866	842	814
z=30	796	795	792	787	780	770	757	743	725	705	681
z=35	639	638	636	631	625	617	607	595	581	564	545
z=40	494	493	491	488	483	476	469	459	448	435	421
z=45	371	371	369	366	363	358	352	345	336	327	316
z=50	274	274	273	271	268	264	260	255	249	242	234
z=55	202	201	200	199	197	194	191	187	183	178	172
z=60	148	148	147	146	145	143	140	138	134	131	127
z=65	109	109	109	108	107	106	104	102	99.7	97.1	94.3
z=70	81.6	81.5	81.2	80.6	79.8	78.9	77.6	76.2	74.6	72.8	70.8
z=75	61.6	61.5	61.2	60.8	60.3	59.6	58.7	57.7	56.5	55.2	53.8
z=80	47	46.9	46.8	46.5	46.1	45.5	44.9	44.2	43.3	42.4	41.4
z=85	36.3	36.3	36.1	35.9	35.6	35.2	34.8	34.3	33.6	33	32.2
z=90	28.4	28.3	28.3	28.1	27.9	27.6	27.3	26.9	26.4	25.9	25.4
z=95	22.5	22.4	22.4	22.2	22.1	21.9	21.6	21.3	21	20.6	20.3
z=100	18	17.9	17.9	17.8	17.7	17.5	17.4	17.1	16.9	16.6	16.3

y=2	x=0	x=2	x=4	x=6	x=8	x=10	x=12	x=14	x=16	x=18	x=20
z=0	1327	1325	1320	1312	1300	1284	1264	1240	1211	1177	1137
z=5	1313	1311	1306	1298	1286	1271	1251	1227	1198	1164	1125
z=10	1270	1269	1264	1256	1244	1229	1210	1187	1159	1127	1089
z=15	1196	1195	1190	1183	1172	1158	1140	1118	1092	1061	1026
z=20	1089	1088	1084	1077	1067	1054	1038	1018	994	966	934
z=25	953	952	948	942	934	922	908	890	869	845	817
z=30	798	797	794	788	781	771	759	744	727	706	683
z=35	639	638	635	631	625	617	607	595	581	565	546
z=40	493	492	490	486	482	475	468	458	447	435	420
z=45	370	369	368	365	361	356	350	343	335	326	315
z=50	273	273	271	269	267	263	259	253	247	240	233
z=55	200	200	199	198	196	193	190	186	182	177	171
z=60	147	147	146	145	144	142	139	137	134	130	126
z=65	109	109	108	107	106	105	103	101	99	96.5	93.7
z=70	81.1	81	80.7	80.1	79.4	78.4	77.2	75.8	74.2	72.4	70.4
z=75	61.2	61.1	60.9	60.5	59.9	59.2	58.4	57.3	56.2	54.9	53.5
z=80	46.7	46.7	46.5	46.2	45.8	45.3	44.7	43.9	43.1	42.2	41.2
z=85	36.1	36.1	36	35.7	35.4	35.1	34.6	34.1	33.5	32.8	32.1
z=90	28.3	28.2	28.1	28	27.8	27.5	27.1	26.8	26.3	25.8	25.3
z=95	22.4	22.3	22.3	22.2	22	21.8	21.5	21.3	20.9	20.6	20.2
z=100	17.9	17.9	17.8	17.7	17.6	17.5	17.3	17.1	16.8	16.6	16.3

y=4	x=0	x=2	x=4	x=6	x=8	x=10	x=12	x=14	x=16	x=18	x=20
z=0	1338	1337	1332	1324	1312	1296	1277	1253	1224	1190	1151
z=5	1325	1323	1318	1310	1299	1283	1264	1240	1212	1178	1139
z=10	1282	1281	1276	1268	1257	1242	1224	1201	1173	1141	1103
z=15	1208	1207	1203	1195	1185	1171	1153	1132	1106	1075	1040
z=20	1101	1099	1095	1089	1079	1066	1050	1031	1007	979	947
z=25	962	960	957	951	942	931	917	900	879	855	827
z=30	802	801	798	792	785	776	764	749	732	711	688
z=35	638	637	635	631	625	617	607	595	581	565	546
z=40	489	488	486	483	478	472	464	455	444	432	418
z=45	365	364	363	360	357	352	346	339	331	322	311
z=50	268	268	267	265	262	259	254	249	243	236	229
z=55	196	196	195	194	192	189	186	182	178	173	168
z=60	144	144	143	142	141	139	137	134	131	128	124
z=65	107	106	106	105	104	103	101	99.3	97.1	94.7	92
z=70	79.6	79.5	79.2	78.7	77.9	76.9	75.8	74.4	72.8	71.1	69.1
z=75	60.2	60.1	59.8	59.4	58.9	58.2	57.4	56.4	55.2	54	52.6
z=80	46	45.9	45.8	45.5	45.1	44.6	44	43.2	42.4	41.5	40.5
z=85	35.6	35.6	35.4	35.2	34.9	34.6	34.1	33.6	33	32.3	31.6
z=90	27.9	27.8	27.8	27.6	27.4	27.1	26.8	26.4	26	25.5	25
z=95	22.1	22.1	22	21.9	21.7	21.5	21.3	21	20.7	20.3	19.9
z=100	17.7	17.7	17.6	17.5	17.4	17.3	17.1	16.9	16.6	16.4	16.1

y=6	x=0	x=2	x=4	x=6	x=8	x=10	x=12	x=14	x=16	x=18	x=20
z=0	1357	1356	1351	1343	1332	1317	1298	1275	1247	1213	1174
z=5	1344	1343	1338	1330	1319	1304	1286	1263	1235	1202	1163
z=10	1303	1301	1297	1289	1279	1264	1246	1224	1197	1165	1127
z=15	1229	1228	1224	1217	1206	1193	1176	1155	1130	1099	1064
z=20	1120	1119	1115	1108	1099	1087	1071	1052	1029	1001	969
z=25	976	975	971	966	957	947	933	916	896	872	844
z=30	808	807	804	799	792	783	772	757	740	720	697
z=35	637	636	634	630	624	616	607	595	582	566	547
z=40	482	482	480	477	472	466	459	450	439	427	413
z=45	356	356	354	352	349	344	338	332	324	315	305
z=50	260	260	259	257	255	251	247	242	236	230	222
z=55	190	190	189	188	186	183	180	177	172	168	163
z=60	139	139	139	138	136	134	132	130	127	123	120
z=65	103	103	103	102	101	99.5	98	96.1	94	91.6	89
z=70	77.2	77.1	76.8	76.2	75.5	74.6	73.4	72.1	70.6	68.9	67
z=75	58.4	58.3	58.1	57.7	57.2	56.5	55.7	54.8	53.7	52.4	51.1
z=80	44.8	44.7	44.5	44.3	43.9	43.4	42.8	42.1	41.3	40.4	39.5
z=85	34.7	34.7	34.6	34.4	34.1	33.7	33.3	32.8	32.2	31.6	30.9
z=90	27.3	27.2	27.1	27	26.8	26.5	26.2	25.8	25.4	24.9	24.4
z=95	21.6	21.6	21.6	21.5	21.3	21.1	20.9	20.6	20.3	19.9	19.5
z=100	17.4	17.4	17.3	17.2	17.1	17	16.8	16.6	16.4	16.1	15.8

y=8	x=0	x=2	x=4	x=6	x=8	x=10	x=12	x=14	x=16	x=18	x=20
z=0	1384	1382	1378	1371	1360	1346	1328	1306	1279	1246	1207
z=5	1371	1370	1365	1358	1348	1334	1316	1294	1267	1235	1196
z=10	1331	1330	1326	1319	1308	1295	1278	1256	1230	1199	1162
z=15	1258	1257	1253	1247	1237	1224	1208	1188	1163	1134	1099
z=20	1147	1146	1142	1136	1128	1116	1101	1083	1060	1033	1001
z=25	996	995	992	987	979	969	956	939	920	896	868
z=30	817	816	813	809	802	793	782	769	752	733	710
z=35	634	633	631	627	622	615	606	595	582	566	548
z=40	472	472	470	467	463	457	450	442	432	420	406
z=45	344	344	342	340	337	333	327	321	313	305	295
z=50	249	249	248	246	244	240	237	232	226	220	213
z=55	181	181	180	179	177	175	172	168	164	160	155
z=60	133	133	132	131	130	128	126	123	121	117	114
z=65	98.3	98.2	97.8	97.1	96.1	94.9	93.4	91.7	89.6	87.4	84.9
z=70	73.8	73.7	73.4	72.9	72.2	71.3	70.2	68.9	67.5	65.9	64.1
z=75	56	55.9	55.7	55.4	54.9	54.2	53.4	52.5	51.5	50.3	49
z=80	43.1	43	42.9	42.6	42.2	41.8	41.2	40.5	39.8	38.9	38
z=85	33.5	33.5	33.4	33.2	32.9	32.6	32.2	31.7	31.1	30.5	29.8
z=90	26.4	26.4	26.3	26.1	26	25.7	25.4	25	24.6	24.2	23.7
z=95	21	21	20.9	20.8	20.7	20.5	20.3	20	19.7	19.4	19
z=100	16.9	16.9	16.9	16.8	16.7	16.5	16.4	16.2	15.9	15.7	15.4

y=10	x=0	x=2	x=4	x=6	x=8	x=10	x=12	x=14	x=16	x=18	x=20
z=0	1417	1416	1412	1405	1396	1383	1366	1345	1320	1288	1250
z=5	1405	1404	1400	1393	1384	1371	1355	1334	1309	1277	1240
z=10	1367	1366	1362	1356	1347	1335	1319	1299	1274	1244	1207
z=15	1296	1295	1292	1286	1277	1266	1251	1232	1208	1180	1145
z=20	1183	1182	1179	1174	1166	1155	1141	1124	1103	1077	1045
z=25	1023	1022	1019	1015	1008	998	986	971	952	929	902
z=30	828	827	825	821	815	807	797	784	768	749	727
z=35	629	629	626	623	618	612	603	593	581	566	548
z=40	458	457	456	453	449	444	437	430	420	409	396
z=45	328	327	326	324	321	317	312	306	299	291	282
z=50	234	234	233	232	229	226	223	218	213	207	201
z=55	169	169	169	167	166	163	161	158	154	150	145
z=60	124	124	123	123	121	120	118	116	113	110	107
z=65	92.3	92.1	91.7	91.1	90.2	89.1	87.7	86	84.1	82	79.7
z=70	69.5	69.4	69.1	68.6	68	67.2	66.1	65	63.6	62.1	60.4
z=75	53	53	52.7	52.4	51.9	51.3	50.6	49.7	48.7	47.6	46.4
z=80	41	40.9	40.8	40.5	40.2	39.7	39.2	38.6	37.8	37	36.2
z=85	32	32	31.9	31.7	31.5	31.1	30.7	30.3	29.7	29.2	28.5
z=90	25.3	25.3	25.2	25.1	24.9	24.7	24.4	24	23.6	23.2	22.7
z=95	20.3	20.2	20.2	20.1	19.9	19.8	19.5	19.3	19	18.7	18.3
z=100	16.4	16.4	16.3	16.2	16.1	16	15.8	15.6	15.4	15.2	14.9

4. Magnetic field measurement

In this measurement we used 3MH3: 3-Axis Digital Teslameter [12]. This tesla meter has a three-axis Hall probe, which is fixed on an x-y stage. The probe head has 4 mm width, 2 mm thickness, and 15 mm length. The field sensitive area is 0.15 mm x 0.01 mm x 0.15 mm. The measurement range along z-axis is from -100 mm to 100 mm with 4 mm steps. X and Y-coordinates of the measurement lines are from -6 mm to 6 mm with 2 mm steps. We also measured additional points on four lines of (x, y) = {(-10, -10), (-10, 10), (10, -10), (10, 10)}. The alignment error on the magnet against the x-y stage axis is less than 0.1mm.

Results of the magnetic field By is shown in Table 2. Those of Bx and Bz are shown in Table 3 and 4, respectively. These values are calibrated using a NMR probe. And in this measurement, the room temperature is changed from 19.0 to 19.3 degree C. The values are also calibrated using with temperature coefficient (TC). A TC of the probe is $1*10^{-3}$ / degree C. A result of BLy integrated along z-axis is shown in Table 5. Those of BLx and BLz are shown in Table 6 and 7, respectively. These BL values are calculated by Simpson's formula. Figure 13 shows the y-component of the magnetic flux density along z-axis on x = y = 0 and x = y = 10. Figure 14 shows the same information as Fig. 13 on x = y = 10 and x = y = -10. Figure 15 and 16 show the x and y component of the magnetic flux density along z-axis on x = y = 0 and x = y = 10, respectively.

Differences between experimental data and calculated data are shown in Figs. 17a, 18a, 19a, 20a, 21a, and 22a following Eq. (8).

$$Difference = (Calculated\ Value) - (Measured\ Value) \qquad (8)$$

The differences are plotted in % at Figs. 17b, 18b, 19b, 20b, 21b, and 22b following Eq. (9).

$$Difference\ \ in\,\% = \frac{(Calculated\ Value) - (Measured\ Value)}{(Calculated\ Value)} \times 100 \qquad (9)$$

The difference and difference in % of By along z-axis on x = y = 0, x = y = 10, and x = y = -10 are shown in Fig. 17, 18, and 19, respectively. Those of Bx on x = y = 10 and x = y = -10 are shown in Fig. 20 and Fig. 21, respectively. The difference of Bz on x = y = 10 is shown in Fig. 22.

The calculated data of Bz has 0 value at z = 0. Differences of BL values are also calculated. The results of these are shown in Table 8.

The positioning angle accuracy of the Hall probe may have some errors, since the Bx and Bz component should be zero on the axis because of the symmetry, while the measured values have none zeros. According to the (Bx, By, Bz) values (15, -32, 1323) Gauss at the center, the rolling and the tilt angles are estimated as 0.65 degree and1.4 degree, respectively. The angle positioning of such a small device is not easy in the measurement.

5. Summary

We fabricated a permanent magnet employing neodymium pieces to get better signal to noise ratio to find long-lived $\pi^+\pi^-$ atoms. The maximum magnetic field strength at the center was 1323 Gauss with the gap of 60 mm which was requied by the beam halo interference to the magnet. The maximum field strength is within the allowed value not to quench the long-lived excited $\pi^+\pi^-$ atoms to the ground state. The magnetic field along the tracks is diminished enough at 10cm from the production target of Be, where the platinum foil is set not to bend the π^+ and π^- tracks after the break-up of the long-lived $\pi^+\pi^-$ atoms, while keeping the bending power BLy of 0.01T.m.

There are small differences between the simulated and the realized field strength as shown in Figs. 17 – 22, but the differences are not large problem in the bending function. The maximum field strength at the center and the bending power of BLy are consistent within 1.7 % and 0.02 %, respectively. In conclusion the magnet was fabricated to fulfill the requirements in Dirac experiment to find the long-lived $\pi^+\pi^-$ atoms.

Table 2: *Magnetic field map of By measured by 3MH3: 3-Axis Digial Teslameter. Units are in Gauss and mm.*

(x, y) = (0, 0) and (10, 10)

z , x=y= 0	By	z , x=y=0	By	z , x=y=10	By	z , x=y=10	By
-100	18	4	1310	-100	13	4	1369
-96	22	8	1280	-96	20	8	1343
-92	25	12	1229	-92	23	12	1297
-88	32	16	1161	-88	26	16	1226
-84	38	20	1073	-84	31	20	1132
-80	45	24	967	-80	39	24	1005
-76	59	28	846	-76	51	28	857
-72	75	32	721	-72	62	32	701
-68	93	36	595	-68	77	36	546
-64	119	40	483	-64	95	40	418
-60	152	44	382	-60	122	44	317
-56	194	48	300	-56	156	48	238
-52	247	52	234	-52	204	52	183
-48	319	56	182	-48	266	56	140
-44	405	60	140	-44	351	60	112
-40	509	64	109	-40	465	64	86
-36	628	68	87	-36	606	68	68
-32	756	72	68	-32	771	72	55
-28	883	76	55	-28	936	76	45
-24	1006	80	44	-24	1094	80	36
-20	1112	84	36	-20	1213	84	28
-16	1195	88	26	-16	1296	88	26
-12	1257	92	25	-12	1349	92	21
-8	1299	96	20	-8	1375	96	16
-4	1320	100	15	-4	1385	100	13
0	1323			0	1384		

Table 3: *Magnetic field map of Bx measured by 3MH3: 3-Axis Digial Teslameter. Units are in Gauss and mm.*

(x, y) = (0, 0) and (10, 10)

z, x=y =0	Bx	z, x=y = 0	Bx	z , x=y = 10	Bx	z, x=y=10	Bx
-100	-1	4	15	-100	-2	4	102
-96	-2	8	15	-96	0	8	101
-92	0	12	13	-92	0	12	96
-88	-2	16	11	-88	2	16	89
-84	0	20	10	-84	3	20	82
-80	-1	24	11	-80	3	24	73
-76	-2	28	9	-76	3	28	62
-72	1	32	8	-72	5	32	54
-68	2	36	4	-68	7	36	43
-64	0	40	3	-64	10	40	33
-60	1	44	3	-60	12	44	26
-56	1	48	2	-56	18	48	22
-52	3	52	2	-52	21	52	17
-48	3	56	2	-48	26	56	12
-44	5	60	0	-44	35	60	8
-40	6	64	0	-40	44	64	7
-36	8	68	0	-36	52	68	5
-32	8	72	-1	-32	62	72	3
-28	11	76	-1	-28	71	76	3
-24	11	80	-1	-24	79	80	0
-20	13	84	-2	-20	88	84	0
-16	13	88	0	-16	94	88	0
-12	13	92	-13	-12	99	92	0
-8	13	96	-1	-8	103	96	0
-4	16	100	-1	-4	105	100	-2
0	15			0	105		

Table 4: *Magnetic field map of Bz measured by 3MH3: 3-Axis Digial Teslameter. Units are in Gauss and mm.*

(x, y) = (0, 0) and (10, 10)

z , x=y=0	Bz	z , x=y= 0	Bz	z , x=y= 10	Bz	z , x= y= 10	Bz
-100	-1	4	-35	-100	18	4	-88
-96	11	8	-33	-96	18	8	-129
-92	-1	12	-33	-92	21	12	-177
-88	0	16	-32	-88	26	16	-230
-84	-1	20	-30	-84	28	20	-281
-80	0	24	-27	-80	35	24	-331
-76	0	28	-24	-76	40	28	-355
-72	11	32	-20	-72	46	32	-355
-68	0	36	-15	-68	62	36	-328
-64	11	40	-12	-64	76	40	-282
-60	11	44	-9	-60	95	44	-230
-56	12	48	-6	-56	124	48	-180
-52	12	52	-3	-52	158	52	-140
-48	11	56	-2	-48	200	56	-106
-44	12	60	-2	-44	250	60	-81
-40	13	64	-1	-40	298	64	-62
-36	0	68	-2	-36	341	68	-48
-32	-1	72	-2	-32	360	72	-38
-28	-8	76	11	-28	347	76	-28
-24	-12	80	-2	-24	300	80	-23
-20	-16	84	-1	-20	232	84	-17
-16	-20	88	0	-16	161	88	-14
-12	-25	92	-1	-12	99	92	-10
-8	-29	96	0	-8	45	96	-10
-4	-30	100	0	-4	-10	100	-7
0	-32			0	-49		

Table 5: *Magnetic field map of Bly which is integrated along z-axis. Units of BL is in Tesla and m. Unit of coordinates is mm.*

x (mm)	y (mm)	BLy (T.m)	x (mm)	y (mm)	BLy (T.m)
-10	-10	0.0098700	2	0	0.0097874
10	-10	0.0098543	4	0	0.0097500
-6	-6	0.0098087	6	0	0.0096791
-4	-6	0.0098636	-6	2	0.0097238
-2	-6	0.0098908	-4	2	0.0097888
0	-6	0.0099019	-2	2	0.0098071
2	-6	0.0098869	0	2	0.0098212
4	-6	0.0098577	2	2	0.0098024
6	-6	0.0097936	4	2	0.0097560
-6	-4	0.0097475	6	2	0.0096922
-4	-4	0.0098075	-6	4	0.0097704
-2	-4	0.0098402	-4	4	0.0098284
0	-4	0.0098409	-2	4	0.0098530
2	-4	0.0098303	0	4	0.0098605
4	-4	0.0097848	2	4	0.0098465
6	-4	0.0097168	4	4	0.0098019
-6	-2	0.0097066	6	4	0.0097372
-4	-2	0.0097674	-6	6	0.0098352
-2	-2	0.0097961	-4	6	0.0098907
0	-2	0.0098067	-2	6	0.0099185
2	-2	0.0097931	0	6	0.0099274
4	-2	0.0097516	2	6	0.0099092
6	-2	0.0096845	4	6	0.0098760
-6	0	0.0097041	6	6	0.0098114
-4	0	0.0097665	-10	10	0.0099217
-2	0	0.0097922	10	10	0.0098679
0	0	0.0098022			

Table 6: *Magnetic field map of BLx which is integrated along z-axis. Units of BLx is in milli-Tesla and m. Unit of coordinates is mm.*

x (mm)	y (mm)	BLx (mT.m)	x (mm)	y (mm)	BLx (mT.m)
-10	-10	0.6722	2	0	0.0907
10	-10	-0.7531	4	0	0.0843
-6	-6	0.2815	6	0	0.0873
-4	-6	0.2071	-6	2	-0.0046
-2	-6	0.1379	-4	2	0.0268
0	-6	0.0680	-2	2	0.0532
2	-6	0.0009	0	2	0.0859
4	-6	-0.2029	2	2	0.1138
6	-6	-0.3117	4	2	0.1339
-6	-4	0.2142	6	2	0.1509
-4	-4	0.1702	-6	4	-0.1864
-2	-4	0.1131	-4	4	-0.0450
0	-4	0.0717	-2	4	0.0320
2	-4	0.0166	0	4	0.0931
4	-4	-0.0243	2	4	0.1417
6	-4	-0.1791	4	4	0.1829
-6	-2	0.1352	6	4	0.2506
-4	-2	0.1179	-6	6	-0.2754
-2	-2	0.1043	-4	6	-0.1438
0	-2	0.0846	-2	6	0.0186
2	-2	0.0607	0	6	0.1008
4	-2	0.0118	2	6	0.1705
6	-2	-0.0050	4	6	0.2480
-6	0	0.0672	6	6	0.3189
-4	0	0.0731	-10	10	-0.6962
-2	0	0.0845	10	10	0.7536
0	0	0.0886			

Table 7: *Magnetic field map of BLz which is integrated along z-axis. Units of BLz is in milli-Tesla and m. Unit of coordinates is mm.*

x (mm)	y (mm)	BLz (mT.m)	x (mm)	y (mm)	BLz (mT.m)
-10	-10	-0.0901	2	0	-0.1559
10	-10	-0.0775	4	0	-0.1358
-6	-6	-0.0892	6	0	-0.1400
-4	-6	-0.0860	-6	2	-0.0883
-2	-6	-0.0880	-4	2	-0.0923
0	-6	-0.0886	-2	2	-0.0911
2	-6	-0.0842	0	2	-0.0937
4	-6	-0.0817	2	2	-0.0930
6	-6	-0.0730	4	2	-0.0923
-6	-4	-0.0770	6	2	-0.0877
-4	-4	-0.0822	-6	4	-0.0770
-2	-4	-0.0896	-4	4	-0.0805
0	-4	-0.0842	-2	4	-0.0854
2	-4	-0.0799	0	4	-0.0906
4	-4	-0.0883	2	4	-0.0846
6	-4	-0.0818	4	4	-0.0852
-6	-2	-0.0918	6	4	-0.0822
-4	-2	-0.1021	-6	6	-0.0817
-2	-2	-0.0947	-4	6	-0.0825
0	-2	-0.0937	-2	6	-0.0905
2	-2	-0.0872	0	6	-0.0945
4	-2	-0.0974	2	6	-0.0909
6	-2	-0.0939	4	6	-0.0860
-6	0	-0.1144	6	6	-0.0875
-4	0	-0.1009	-10	10	-0.0781
-2	0	-0.1168	10	10	-0.0951
0	0	-0.1385			

Table 8: *Differences of BL between calculated data and experimental data.*

	BLx @ x = y = 10 (mT.m) -100 <= z <= 0	BLx @ x = y = 10 (mT.m) -100 <= z <= 100	BLz @ x = y = 10 (mT.m) -100 <= z <= 0	BLy @ x = y = 0 (T.m) -100 <= z <= 0	BLy @ x = y = 0 (T.m) -100 <= z <= 100
Calculated Data	0.3052	0.6329	-1.2946	0.0047160	0.0097848
Experimental Data	0.3837	0.7536	-1.3397	0.0048083	0.0098021
Difference (%)	-27.4	-19.1	-3.5	-2.0	-0.2

	BLy @ x = y = 10 (T.m) -100 <= z <= 0	BLy @ x = y = 10 (T.m) -100 <= z <= 100	BLy @ x = y = -10 (T.m) -100 <= z <= 0	BLy @ x = y = -10 (T.m) -100 <= z <= 100
Calculated Data	0.00473365	0.00983605	0.00473365	0.00983605
Experimental Data	0.00489866	0.00986792	0.00477692	0.00987001
Difference (%)	-3.5	-0.3	-0.9	-0.3

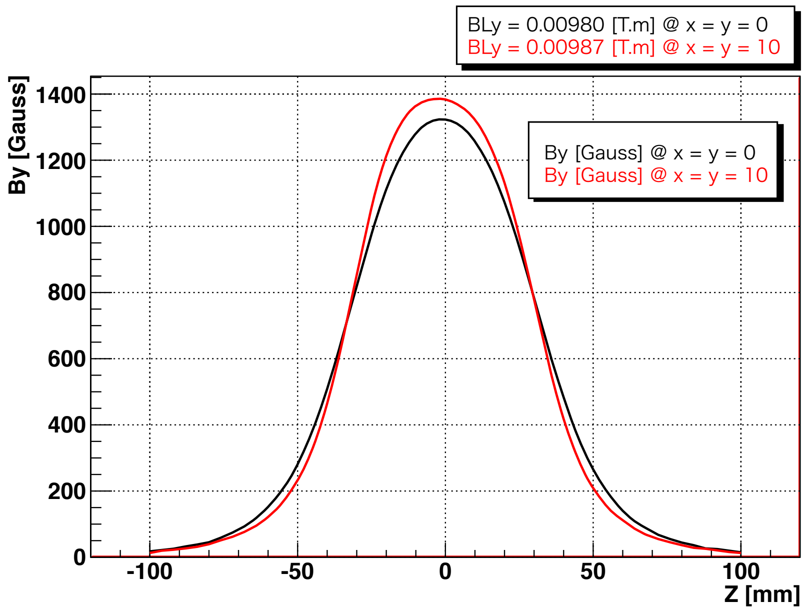

Fig. 13: *Graph of By at (x, y) = (0, 0) and (x, y) = (10, 10). The black line is at x = y = 0. The red line is at x = y = 10.*

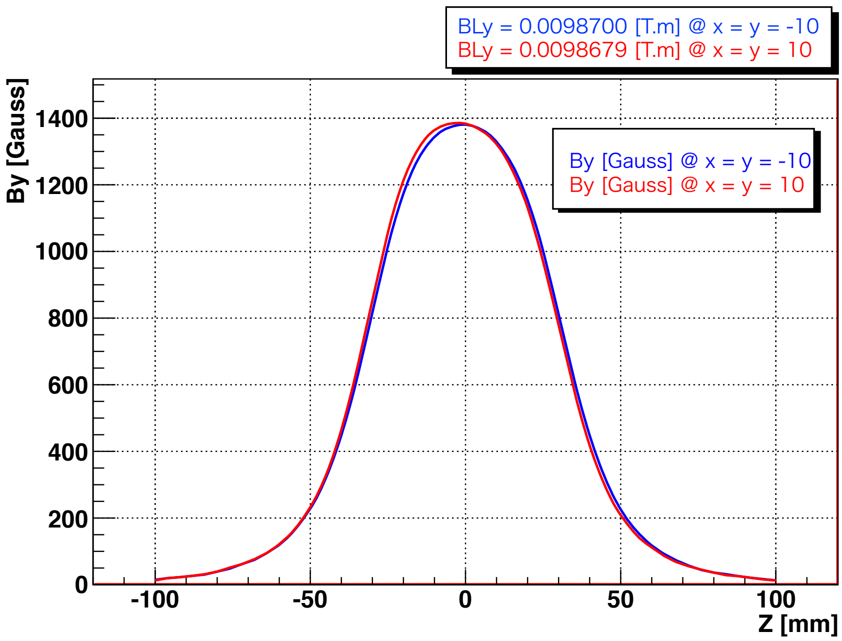

Fig. 14: *Graph of By at (x, y) = (-10, -10) and (x, y) = (10, 10). The blue line is at x = y = -10. The red line is at x = y = 10.*

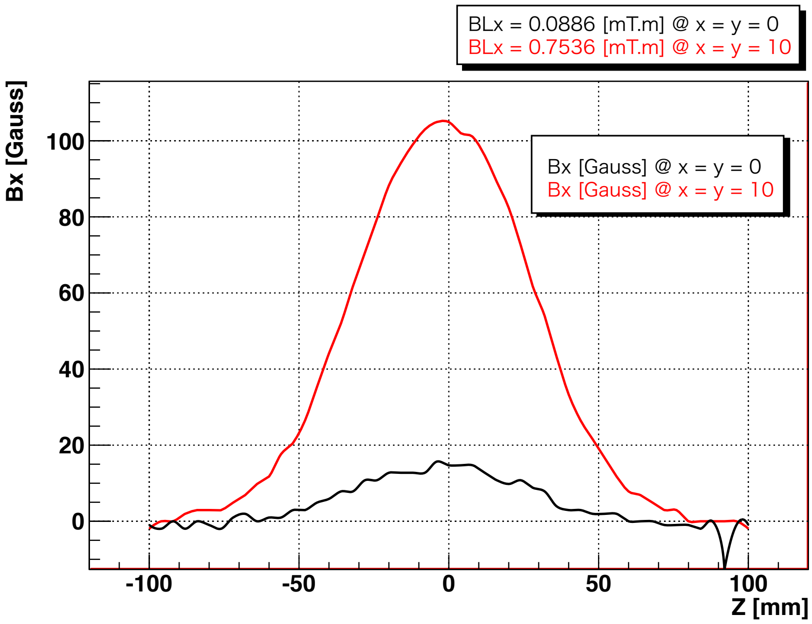

Fig. 15: *Graph of Bx at (x, y) = (0, 0) and (x, y) = (10, 10). The black line is at x = y = 0. The red line is at x = y = 10.*

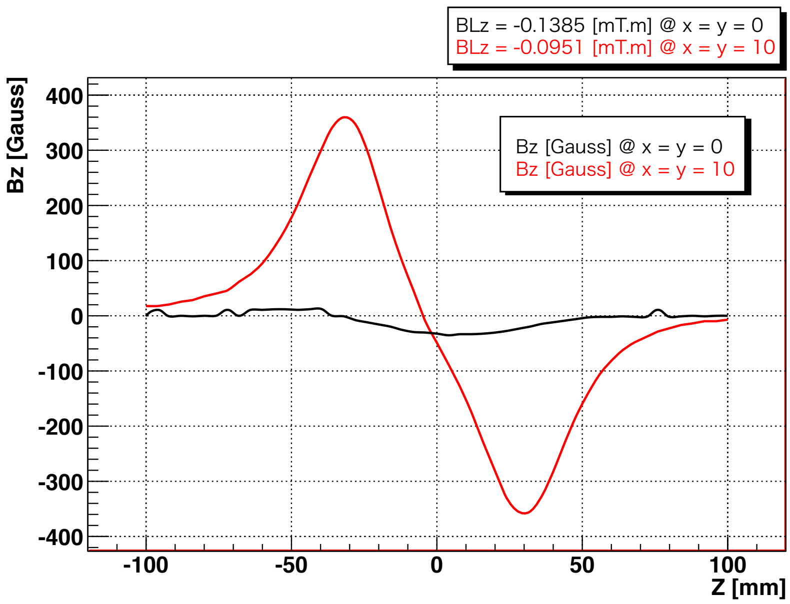

Fig. 16: *Graph of Bz at (x, y) = (0, 0) and (x, y) = (10, 10). The black line is at x = y = 0. The red line is at x = y = 10.*

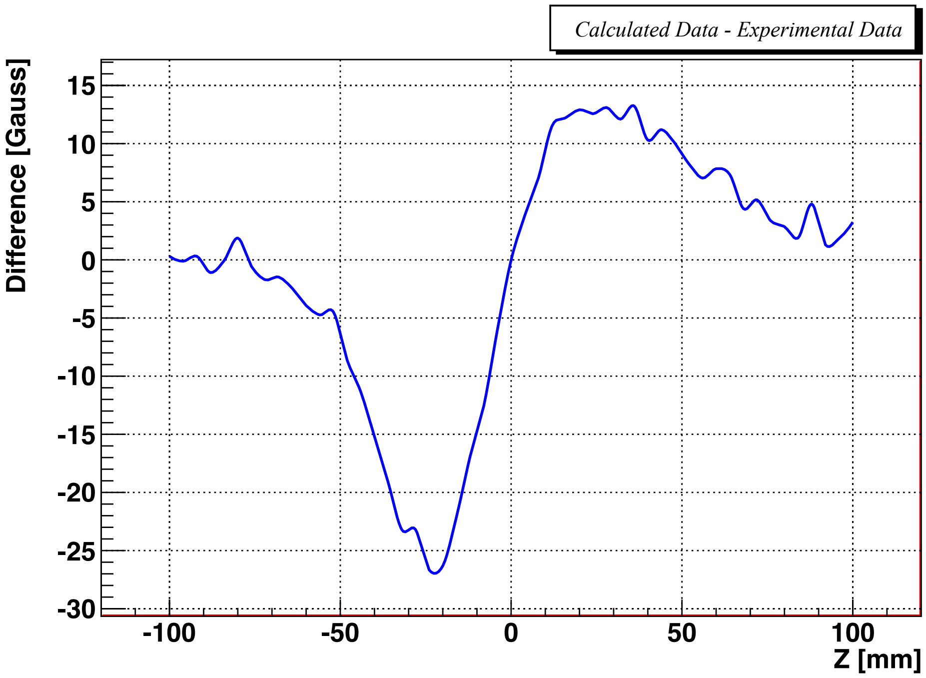

Fig. 17a: *Differences between the calculated By and measured By at x = y = 0.*

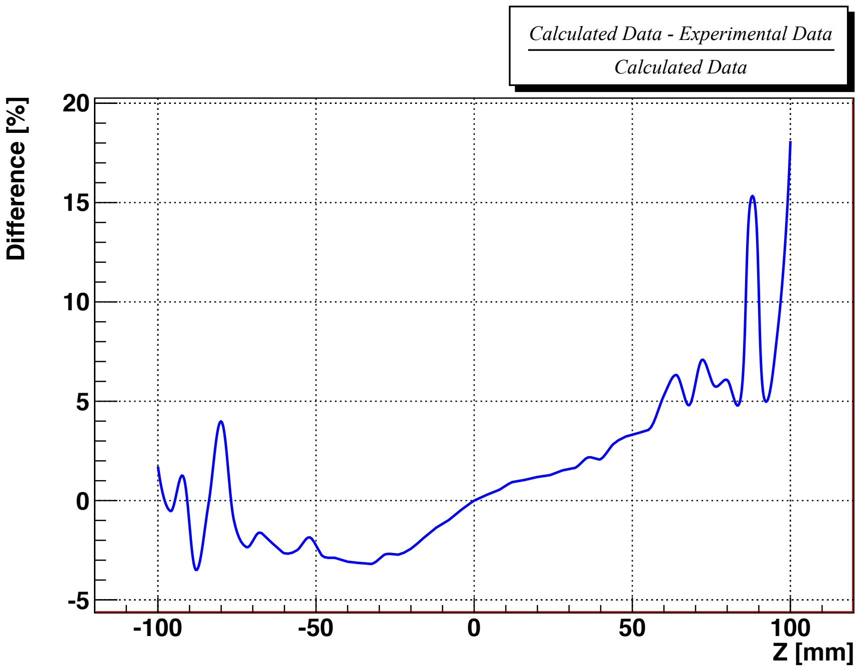

Fig. 17b: *Differences in % between the calculated By and measured By at x = y = 0.*

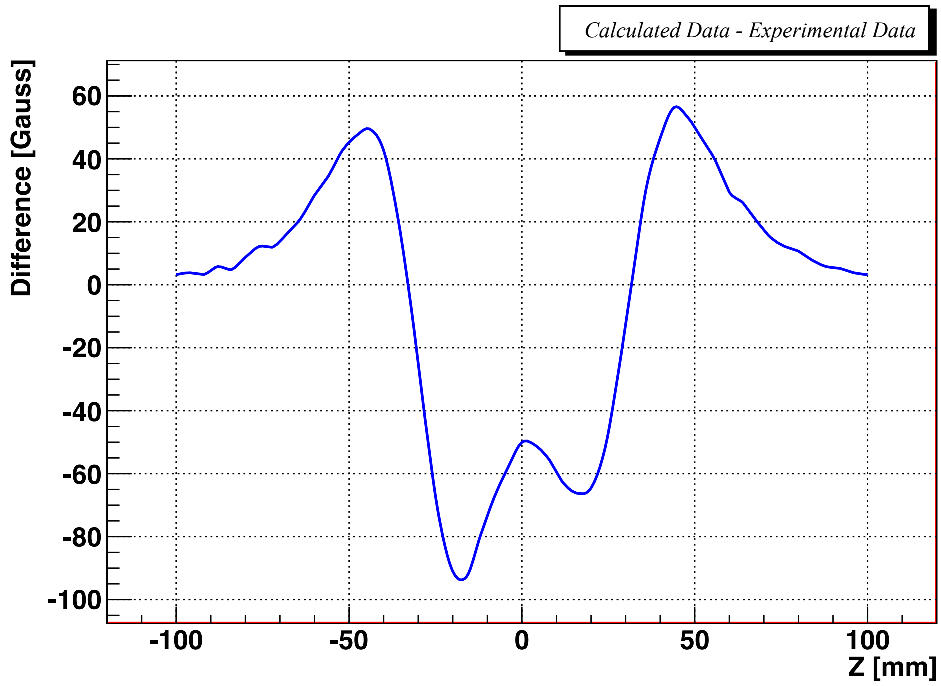

Fig. 18a: *Differences between the calculated By and the measured By at x = y = 10.*

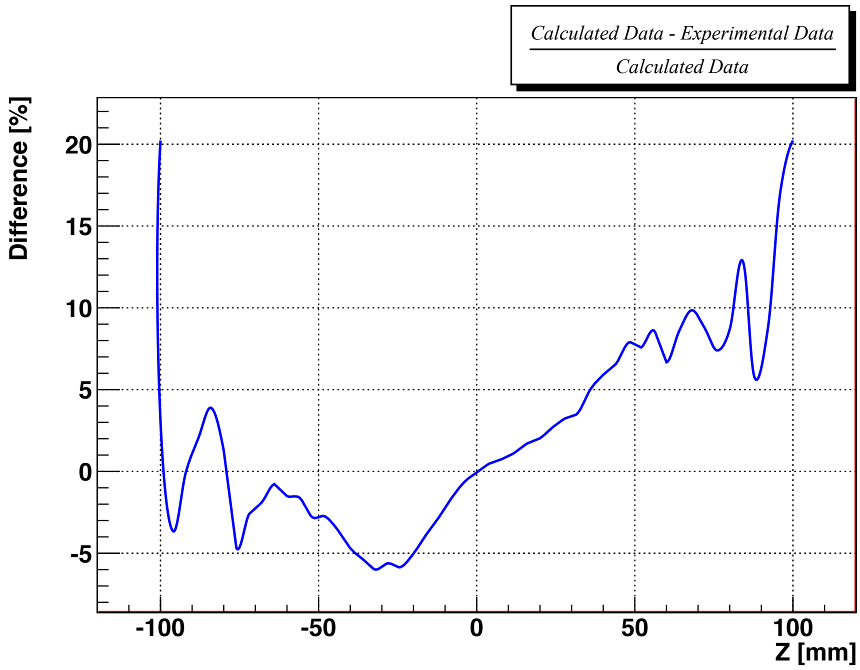

Fig. 18b *Difference in % between the calculated By and the measured By at x = y = 10.*

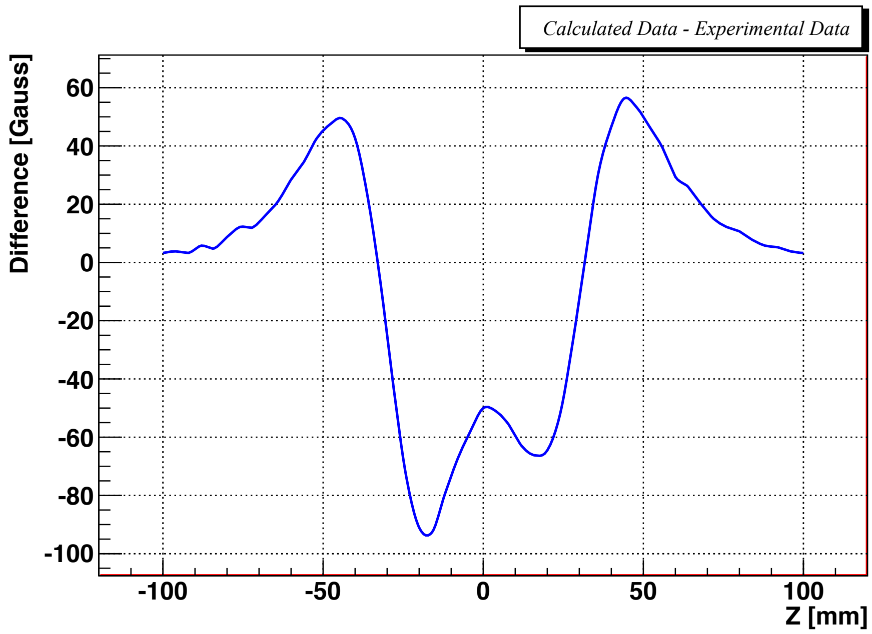

Fig. 19a: *Differences between the calculated By and the measured By at x = y = -10.*

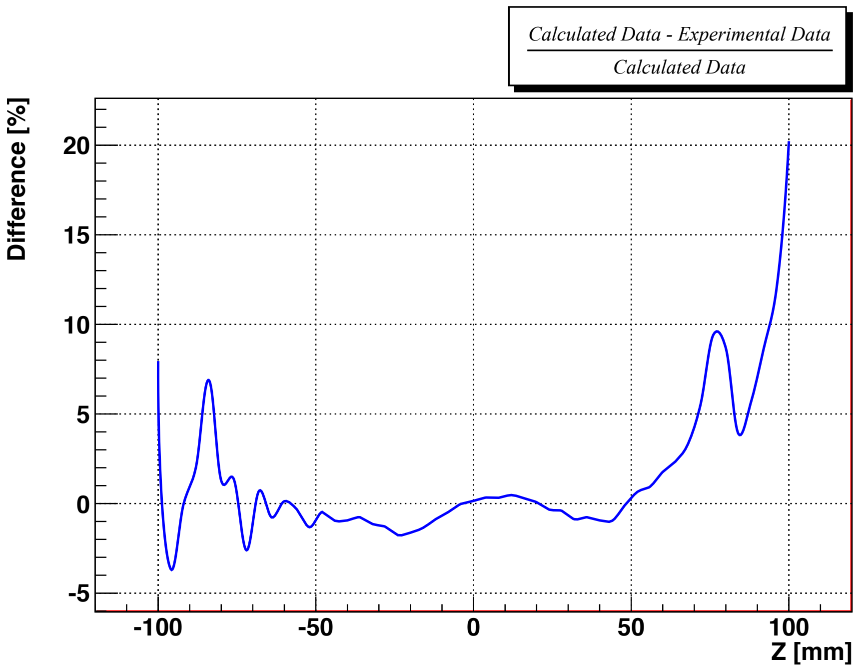

Fig. 19b: *Difference in % between the calculated By and the measured By at x = y = -10.*

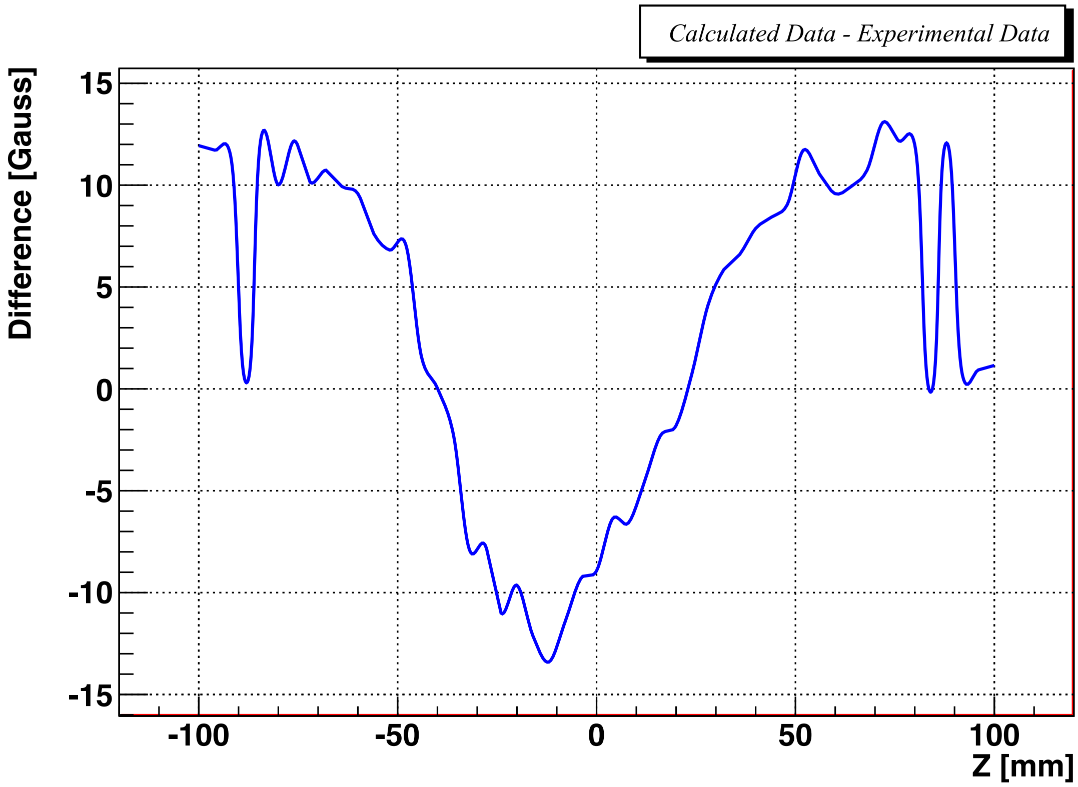

Fig. 20a: *Differences between the calculated Bx and the measured Bx at x = y = 10.*

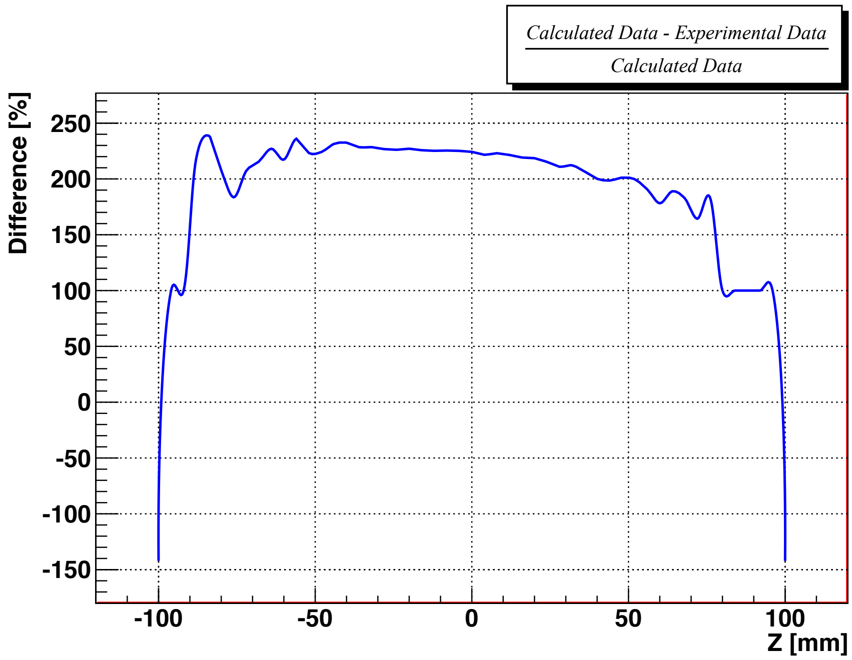

Fig. 20b: *Ddifferences in % between the calculated Bx and the measured Bx at x = y = 10.*

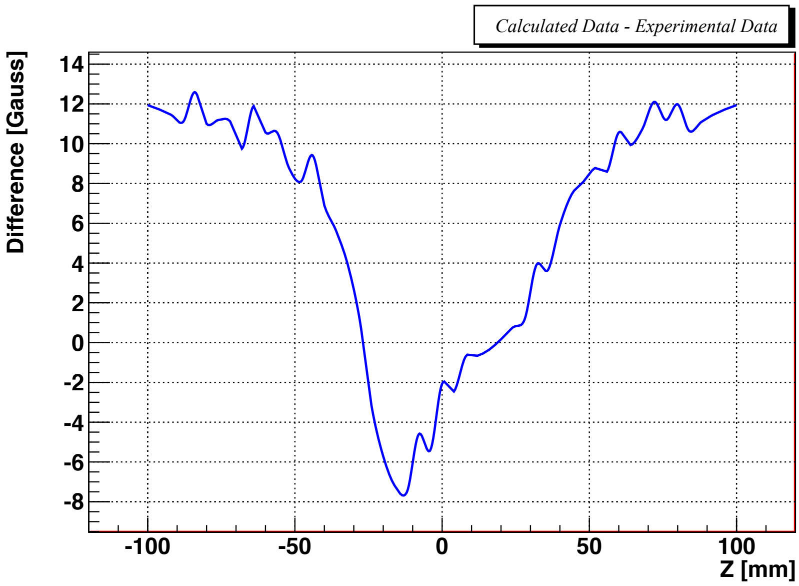

Fig. 21a: *Differences between the calculated Bx and the measured Bx at x = y = -10.*

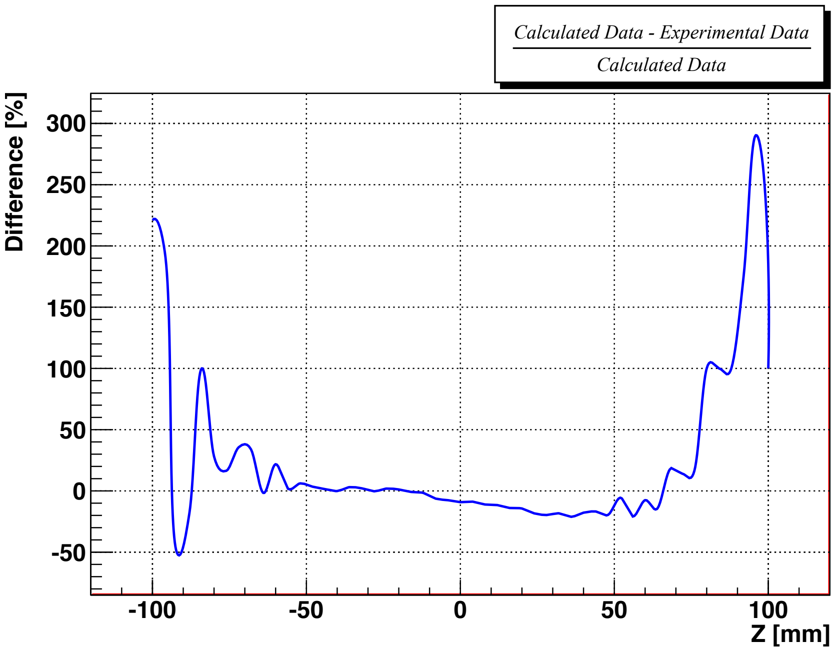

Fig. 21b: *Differencea between the calculated Bx and the measured Bx at x = y = -10.*

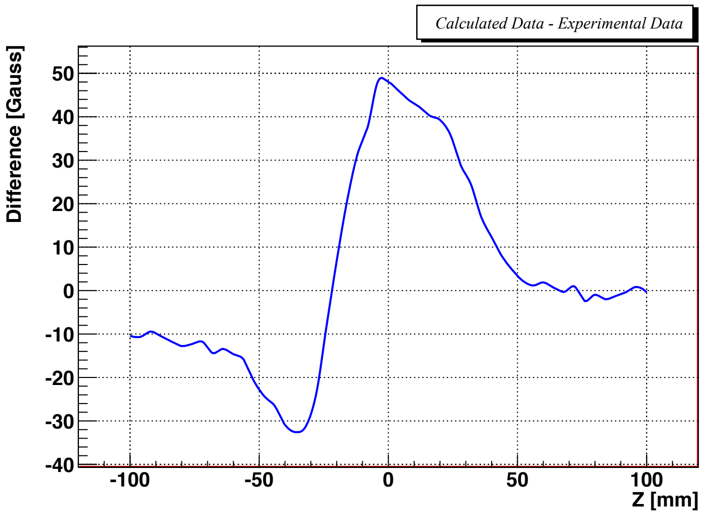

Fig. 22a: *Differences between the calculated Bz and the measured Bz at x = y = 10.*

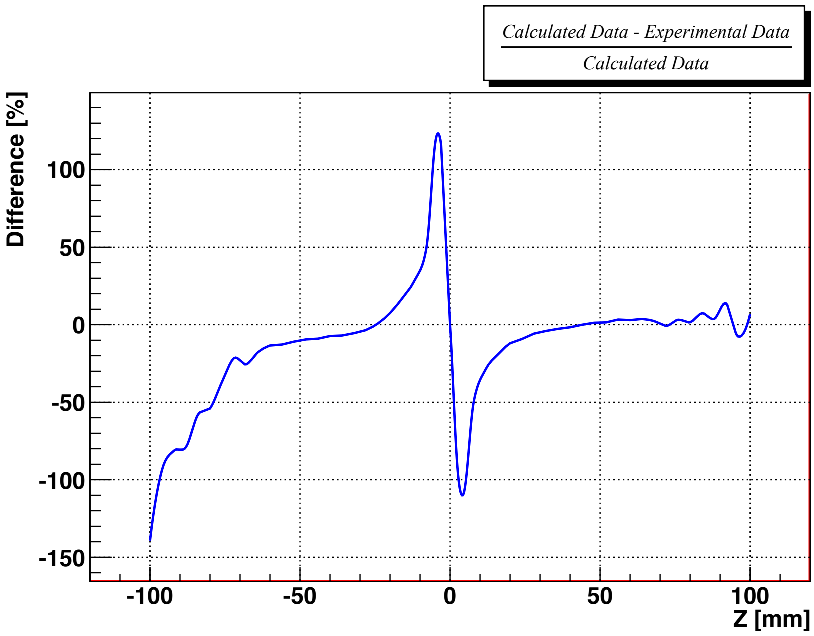

Fig. 22b: *Differences between the calculated Bz and the measured Bz at x = y = 10.*

References

[1] B. Adeva et al, Phys. Lett. B619(2005)50.

[2]B. Adeva et al, CERN-SPSC-2011-001/ SPSC-P-284 Add. 5 January 5, 2011.

[3]M.Chiba, A.Kuptsov and K.Okada, Dirac note 2001-06.

[4]A.Gorin et al., Nucl. Instr. & Meth. in Phys. Res. A566 (2006) 500.

[5]B.Adeva et al., Nucl. Instr. & Meth. in Phys. Res. A515 (2003) 467.

[6] O.-P. Kaehkoenen, S. Maekinen, M. Talvitie and M. Manninen: J. Phys.: Condens. Matter 4 (1992) p.1007-1014.

[7] T. Bizen, T. Tanaka Y. Asano, D. E. Kim, J. S. Bak, H. S. Lee and H. Kitamura: Nucl. Instr. & Meth. in Phys. Res. A467-468 (2001) p.185- 189.

[8] Yoshifumi Ito, Keisuke Yasuda, Ryoya Ishigami, Satoshi Hatori, Osami Okada, Ken Ohashi, and Shintaro Tanaka: Nucl. Instr. And Meth. in Phys. Res. B183 (2001) p.323- 328.

[9] P. Elleaume, O. Chubar, J. Chavanne, "Computing 3D Magnetic Field from Insertion Devices", Proc. of the PAC97 Conference, p.3509-3511.

[10] O. Chubar, P. Elleaume, J. Chavanne, "A 3D Magnetostatics Computer Code for Insertion devices", J. Synchrotron Rad. (1998) 5, p.481-484.

[11] O. Chubar, P. Elleaume, J. Chavanne, C. Benabderrahmane, O. Macouille, F. Marteau, "Application of Finite Volume Integral Approach to Computing of 3D Magnetic Fields Created by Distributed Iron-Dominated Electromagnet Structures", Proc. of the EPAC2004 Conference, p.1675-1677.

[12] http://www.senis.ch/3mh.html